Chemical Science

ROYAL SOCIETY OF CHEMISTRY

EDGE ARTICLE

View Article Online
View Journal | View Issue

Cite this: *Chem. Sci.*, 2020, **11**, 9309

All publication charges for this article have been paid for by the Royal Society of Chemistry

Received 1st June 2020
Accepted 12th August 2020

DOI: 10.1039/d0sc03059g

rsc.li/chemical-science

Stereoretention in styrene heterodimerisation promoted by one-electron oxidants†

Xinglong Zhang ‡[a] and Robert S. Paton *[ab]

Radical cations generated from the oxidation of C=C π-bonds are synthetically useful reactive intermediates for C–C and C–X bond formation. Radical cation formation, induced by sub-stoichiometric amounts of external oxidant, are important intermediates in the Woodward–Hoffmann thermally disallowed [2 + 2] cycloaddition of electron-rich alkenes. Using density functional theory (DFT), we report the detailed mechanisms underlying the intermolecular heterodimerisation of anethole and β-methylstyrene to give unsymmetrical, tetra-substituted cyclobutanes. Reactions between *trans*-alkenes favour the *all-trans* adduct, resulting from a kinetic preference for *anti*-addition reinforced by reversibility at ambient temperatures since this is also the thermodynamic product; on the other hand, reactions between a *trans*-alkene and a *cis*-alkene favour *syn*-addition, while exocyclic rotation in the acyclic radical cation intermediate is also possible since C–C forming barriers are higher. Computations are consistent with the experimental observation that hexafluoroisopropanol (HFIP) is a better solvent than acetonitrile, in part due to its ability to stabilise the reduced form of the hypervalent iodine initiator by hydrogen bonding, but also through the stabilisation of radical cationic intermediates along the reaction coordinate.

1. Introduction

Cyclobutanes are ubiquitous structural motifs in natural products and bioactive molecules.[1,2] They can be considered useful synthons for 3-membered and 5-membered rings *via* regio- and/or stereoselective transformations by ring-contraction or ring-expansion reactions to form otherwise challenging products.[3,4] The inherent ring strain of cyclobutene of 26 kcal mol^{-1} is predominantly due to angular (Baeyer) strain[5] and makes its selective cleavage to access both acyclic and cyclic systems highly amenable. Although the construction of 4-membered cycloalkanes *via* thermal [2 + 2] cycloaddition is symmetry-forbidden based on the Woodward–Hoffmann rules, alternative methods to access this highly versatile motif, with precise chemo-, regio- and stereocontrol continue to emerge. Since the first report of photochemical [2 + 2] cycloaddition accessing a 4-membered carbocycle by Liebermann in 1877,[6] the construction of 4-membered cyclobutyl rings from photo-cycloaddition of alkenes has become arguably the most employed technique for cyclobutanation.[7–12] Cyclobutanation can now also be readily achieved *via* organocatalysis,[13–15] organometallic catalysis,[7,16–18] as well as electrocatalysis[19–22] (Scheme 1). Until recently when the synthesis of substituted cyclobutanes could be realised *via* selective C–H functionalisation of unsubstituted cyclobutanes,[23–26] formal [2 + 2] cycloaddition remained the main strategy for the synthesis of complex, tetra-substituted cyclobutyl rings.[27–30] For the latter strategy, the formation of an unsymmetrical, tetra-substituted cyclobutane can arise from intermolecular heterodimerisation of two substituted alkenes. This, however, remains a challenge as a varied mixture of products can result from the reaction of two alkenes due to a lack of control on homo- and hetero-[2 + 2]-dimerisation and the possibility of regiochemical (head-to-head *vs.* head-to-tail) and stereochemical (*cis vs. trans*) variations. Many examples of both head-to-head and head-to-tail coupled cyclobutanes exist in biologically active natural products, such as argenteoside family of compounds.[31] Synthetic methods for cyclobutane formation with precise control over selectivity are therefore of intense interest.

Radical cations constitute an important class of reactive intermediate in forging C–C and C–X bonds.[32–37] Their formation is typically achieved *via* single-electron transfer (SET) from a neutral substrate's π-bond or lone-pair, creating a "hole" in the system. This process can be mediated using transition metals, either by themselves[7,38–40] or coupled with organic[41] or organometallic[42–45] photoredox catalysts; it can also be mediated by organic oxidants such as aminium radical cationic salts.[46] In this last approach, these powerful oxidants can easily decompose or induce undesirable side reactions.[47–49] Due to

[a]*Department of Chemistry, Chemistry Research Laboratory, University of Oxford, Mansfield Road, Oxford, OX1 3TA, UK*

[b]*Department of Chemistry, Colorado State University, Fort Collins, CO 80523, USA. E-mail: robert.paton@colostate.edu*

† Electronic supplementary information (ESI) available. See DOI: 10.1039/d0sc03059g

‡ Present address: Division of Chemistry and Chemical Engineering, California Institute of Technology, Pasadena, California 91125, USA.

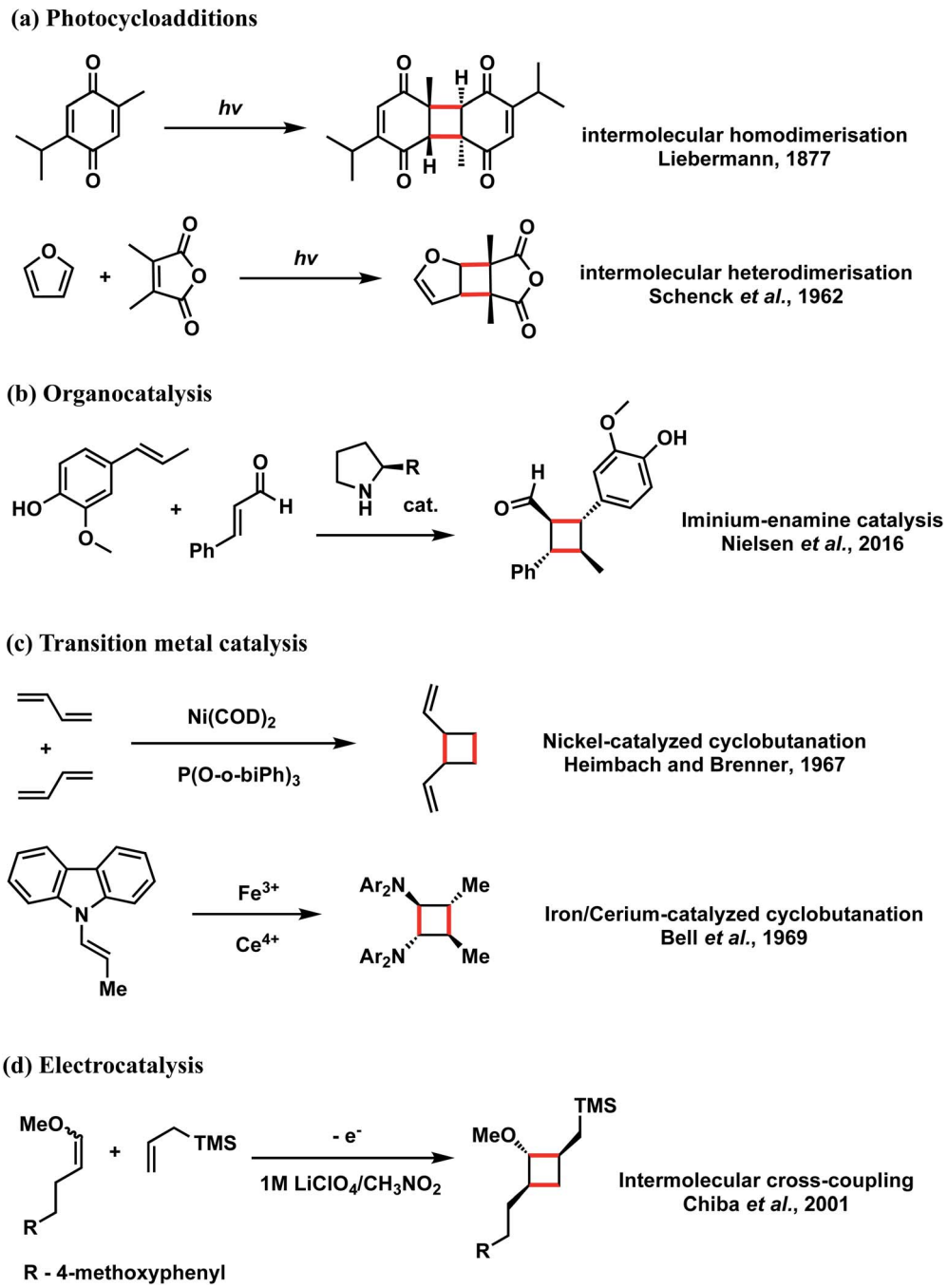

Scheme 1 Selected examples for [2 + 2] cyclobutanation.

these limitations, the use of oxidants for SET-initiation and catalysis of cyclobutanation is very much underexplored compared to photochemical means. In a recent study, Donohoe and co-workers reported the use of a hypervalent iodine oxidants (phenyliodine diacetate or Dess–Martin periodinane (**DMP**)) to promote homo and hetero-dimerisations of styrenes to access unsymmetrical, tetra-substituted cyclobutyl rings.[13,50] The regio- and stereochemical outcomes of this oxidant-promoted, SET-catalysed heterodimerisation of two unsymmetrical alkenes present an interesting avenue for detailed mechanistic study (Scheme 2(a)). The *all-trans* stereochemical outcome of the hypervalent-iodine promoted reaction between *trans*-anethole and *trans*-β-methylstyrene (Scheme 2(a)(i)) is consistent with *trans*-anethole homodimerisation promoted by an aminium cation at temperatures of 0 °C and above (Scheme 2(b)(ii)). At lower temperatures evidence for *cis*-addition is seen (Scheme 2(b)(i)), but complete transfer of alkene stereochemical information occurs at all temperatures. The reaction between *cis*-anethole and *trans*-β-methylstyrene (Scheme 2(b)(iii)), however, shows incomplete stereochemical transfer, giving 20% of the *all-trans* product. Note that in all these products, only the so-called "head-to-head" cyclobutanes are observed.

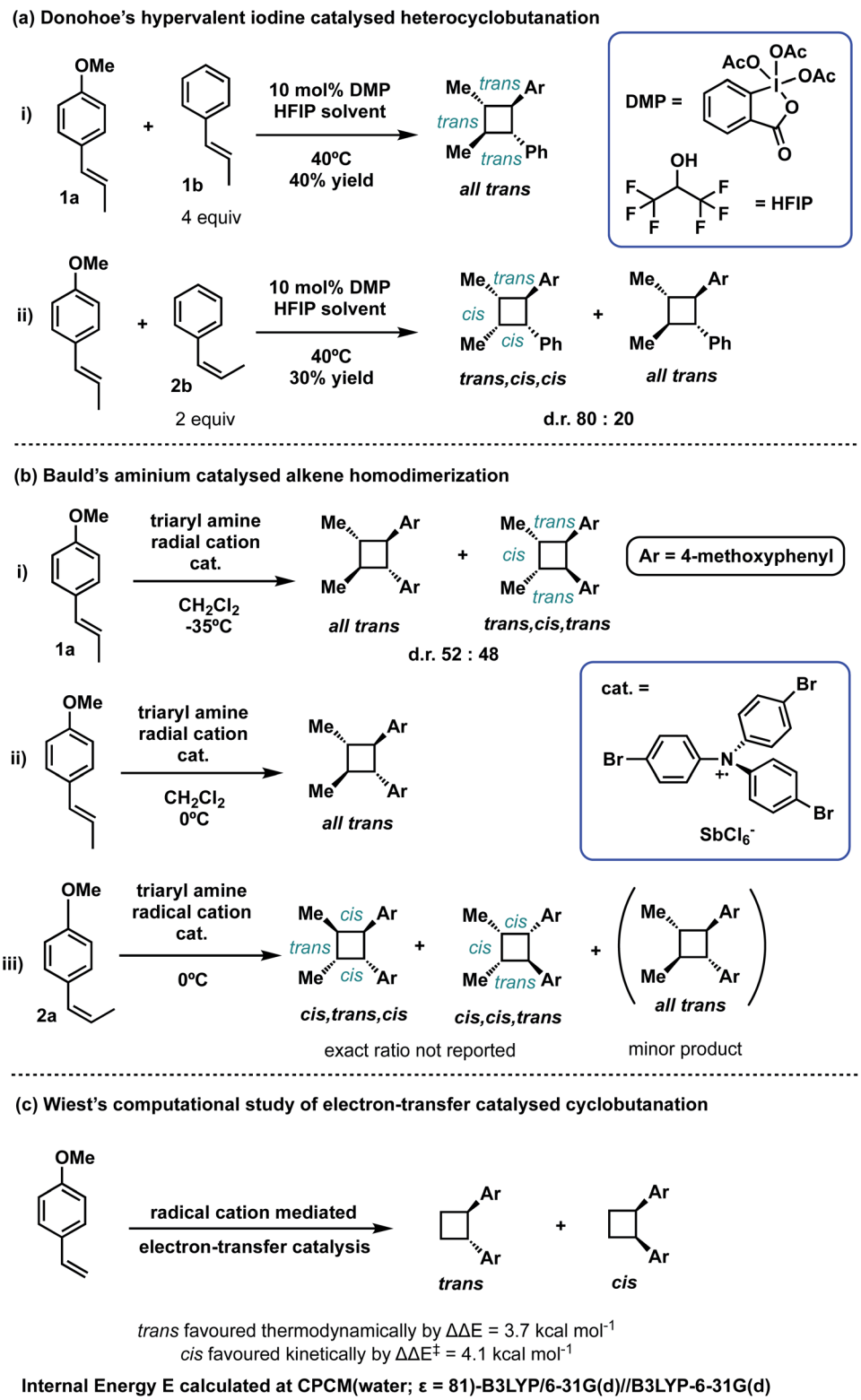

Scheme 2 Stereochemical outcomes from (a) hetero- and (b) homo-coupling of electron-rich alkenes under single electron transfer (SET) catalysis and (c) computational studies of prototypical cyclobutanation from methoxystyrene, a terminal alkene.

The detailed mechanism of intermolecular radical cation cycloaddition has been probed experimentally, where both stepwise[51–54] and concerted, asynchronous[46,55–57] pathways have been proposed. The homo-dimerisation of 4-methoxystyrene to form a disubstituted cyclobutene *via* a radical cationic pathway has been studied computationally (with density

functional theory, DFT) by Wiest and co-workers, where a stepwise mechanism was obtained.[58] The study reported that the *cis*-adduct is favoured kinetically by an activation barrier $\Delta\Delta E^{\ddagger}$ of 4.1 kcal mol^{-1} whereas the *trans*-adduct is favoured thermodynamically by a reaction energy $\Delta\Delta E$ of 3.7 kcal mol^{-1} (Scheme 2(c)). Following this study, Metzger and co-workers in 2008 detected a distonic (where charge and radical sites are separated) radical cationic intermediate *via* extractive electrospray ionisation mass spectrometry, lending direct support to the stepwise mechanism.[59] Further computational mechanistic investigations looking into intramolecular cyclobutanation of (bis)styrene[60] and intermolecular cyclobutanation of unsubstituted styrene[61] *via* radical cation catalysis further confirmed the stepwise nature of such mechanism.

In this computational study, we focus on the effects of alkene *cis*- and *trans*-configurations on the mechanism of the intermolecular radical cation dimerisation of styrenes, since to the best of our knowledge β-substituents have yet to feature in theoretical studies. In the experimental work by Donohoe and co-workers, one particularly intriguing aspect has been the reaction shown in Scheme 2(a)(ii), wherein 20% of *all-trans* cyclobutyl ring product is formed, although the alkenes used do not both have the *trans* geometry. We envisioned that the reaction proceeds *via* initiation, creating a hole in one of the neutral alkenes, followed by propagation, forming radical cationic cyclobutanation, and finally termination, where the radical cationic cyclobutyl product gets reduced to its neutral form (Scheme 3). We herein report a theoretical investigation into the origins governing the chemical reactivities and selectivities effecting the observed stereochemical outcomes in the heterodimerisation of two unsymmetrical, electron-rich alkenes (Scheme 2(a))

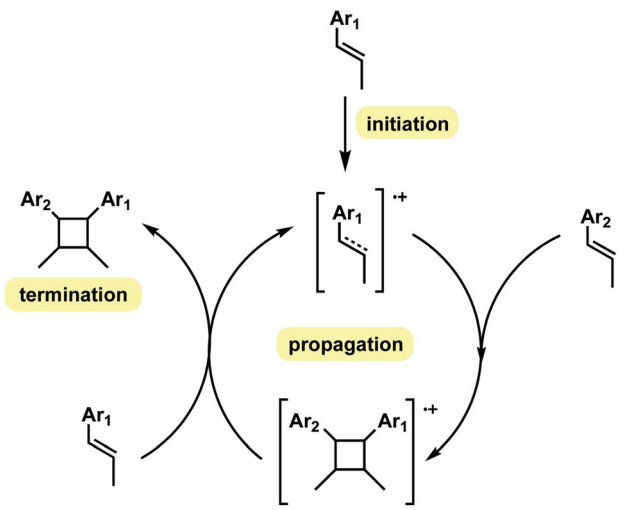

Scheme 3 Schematic outline of catalytic cycle. In the initiation step, one of the alkenes gets oxidised to radical cation, which then attacks the other, neutral alkene to form the radical cationic cyclobutene in the propagation step. The termination step occurs when the radical cationic cyclobutene gets reduced to its neutral form.

2. Results and discussion

2.1 Computational electrochemical potentials

The feasibility of radical cation generation in the initiation step and the reduction of the radical cation product in the termination step can be quantified using the electrochemical potentials of these species. For a reaction between two different alkenes, their electrochemical potentials directly determine their role selectivity as caticogen (one that readily forms radical cation under oxidation/SET conditions) or caticophile (species that attacks the radical cation). The calculation of reduction potentials provides a direct measure of the thermodynamic feasibility of these steps.

Ab initio computations of reduction potentials of various systems have been widely explored.[62–72] We adopt the thermodynamic cycle for redox potential computation[73,74] and found that M06-2X functional gives the best agreement (smallest mean unsigned error, MUE) with the experimental redox potential values for substrates *trans*-anethole **1a** and *trans*-β-methylstyrene **1b** in MeCN solvent amongst 8 functionals tested (ESI section 2†). This is in agreement with a study of both experimental and computational electrochemical potentials for over 180 organic substrates where M06-2X functional gives an R^2 value of 0.97 for the correlation between the experimental and calculated redox potentials.[75] M06-2X was used for all subsequent DFT calculations.

The redox potential of the hypervalent iodine oxidant, Dess–Martin Periodinane (**DMP**, chemical structure in Scheme 2(a)), was computed at SMD(solvent)-M06-2X/def2-TZVPP//M06-2X/GenECP(LanL2DZ for I atom and 6-31G(d) for other atoms) where each of the MeCN and **HFIP** solvents was separately calculated. The results, together with the redox potentials for our starting materials and cyclobutyl ring products, are given in Table 1. From the table, we can see that in both solvents, *trans*-anethole **1a** is oxidised more easily than *trans*-β-methylstyrene **1b** to their respective radical cation. For example, in **HFIP**, the oxidation of **1a** to [**1a**]$^{\bullet+}$ by **DMP** has E_{cell} of 0.306–1.467 = −1.161 V and the oxidation of **1b** to [**1b**]$^{\bullet+}$ has E_{cell} of 0.306–1.879 = −1.573 V, the latter being much less favourable thermodynamically (by about 10 kcal mol^{-1}). Thus, **1a** will act as a caticogen where it is oxidised to its radical cationic form whereas the neutral **1b** will act as a caticophile, attacking the radical cationic [**1a**]$^{\bullet+}$ in the subsequent cyclobutanation steps (*vide infra*).

The effect of solvent has a greater influence on the redox potential of the iodinated oxidant **DMP**, whose reduction potential becomes less negative (by 205 mV) in **HFIP** than in MeCN, indicating its greater oxidising strength in the fluorinated solvent, in agreement with an electrochemical study on the enhanced oxidising power of similar hypervalent iodine oxidants in **HFIP** than in MeCN.[50] The molecular origin of that enhanced reactivity can be traced to the formation of a strong hydrogen-bonded oxidant–**HFIP** complex.[50] By including one molecule of **HFIP** explicitly in our recalculation of redox potentials of **DMP** (see Fig. 1 for optimised structures), we found that the computed redox potential of **DMP** becomes even

Table 1 Computed redox potentials (*V*) of substrates *trans*-anethole **1a**, *trans*-β-methylstyrene **1b**, *cis*-anethole **2a**, *cis*-β-methylstyrene **2b** and hypervalent iodine oxidant Dess–Martin periodinane (**DMP**) and **DMP–HFIP** complex, and the cyclobutyl products (**int3**, **int3′**, **int8** and **int8′**) in MeCN and **HFIP** solvents using M06-2X

	1a	1b	2a	2b	DMP	DMP–HFIP	int3	int3′	Int8	Int8′
Expt[a]	1.484	1.984	—	—	—	—	—	—	—	—
MeCN	1.388	1.815	1.506	1.917	-0.122	0.231	1.676	1.590	1.613	1.669
HFIP	1.467	1.879	1.596	1.988	0.083	0.306	1.754	1.659	1.692	1.744

[a] Value in MeCN solvent and taken from ref. 75.

more positive, being now 223 mV more favoured than without an explicit molecule of **HFIP** (75 mV more favoured in **HFIP** than in MeCN). This can be attributed to the strengthening of the intermolecular H-bond in the **DMP–HFIP** complex upon reduction, with a reduction in the O–H distance from 1.79 to 1.51 Å (Fig. 1). The ease of reduction of **DMP** in MeCN is also augmented by 353 mV by the inclusion of an H-bonded molecule of **HFIP**, although experimentally using **HFIP** as an additive

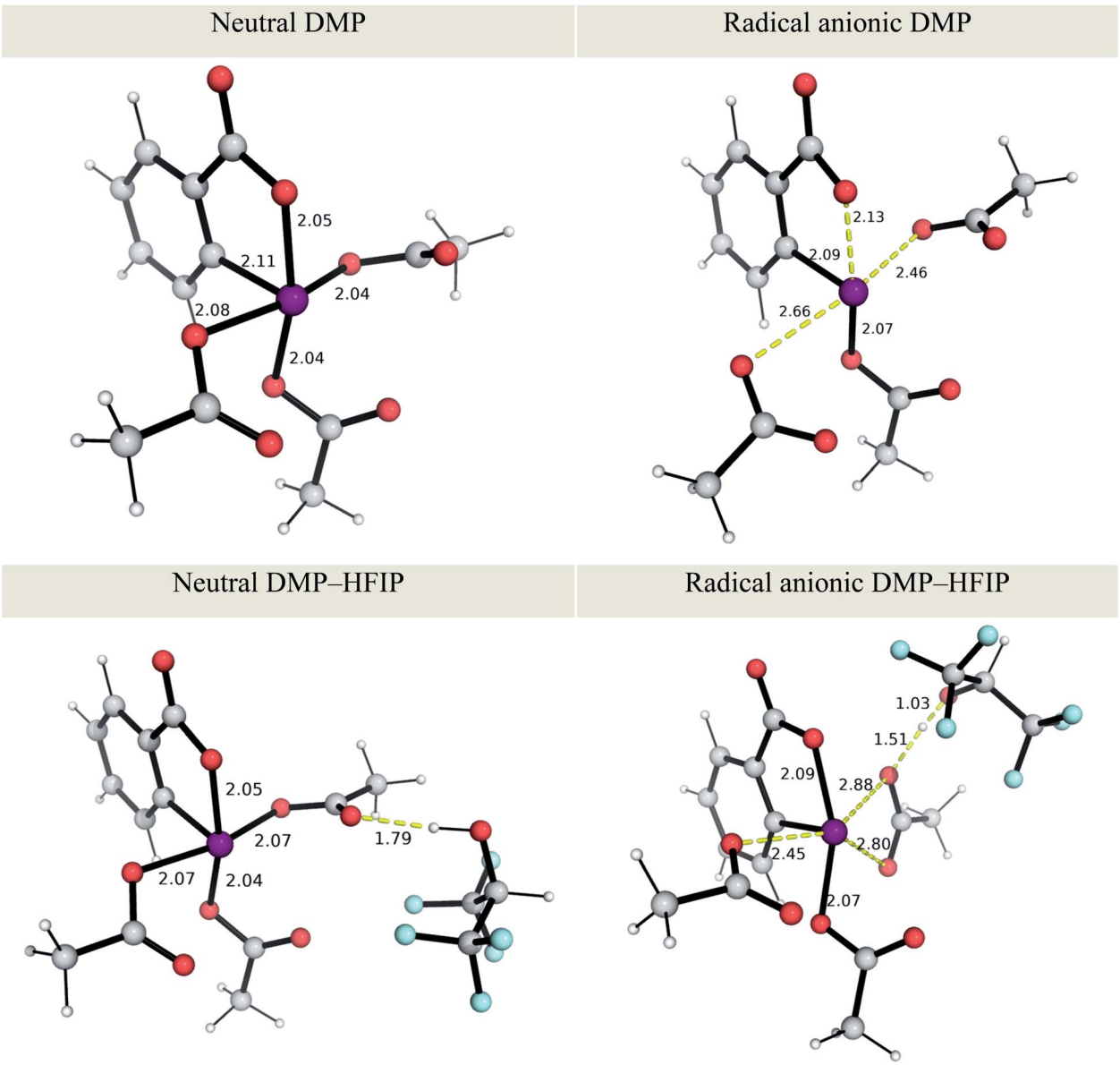

Fig. 1 M06-2X optimised structures of neutral and radical anion forms of Dess–Martin periodinane (**DMP**) and **DMP–HFIP**. See details of conformational considerations in ESI section 2.1.† Key distances are shown in Å.

in MeCN solvent does not lead to significant cyclobutanation (<5% yield) potentially because the MeCN molecule could be a better H-bond acceptor than the hypervalent iodine oxidant for **HFIP** molecule.[50] The formation of radical cationic $[\mathbf{1a}]^{\bullet+}$ can be more easily achieved in **HFIP** (with an overall E_{cell} of 0.306–1.467 = −1.161 V) than in MeCN (overall E_{cell} of −0.122 − 1.388 = −1.510 V without **HFIP**), by *ca.* 8 kcal mol^{-1}, illustrative of the promoting influence of **HFIP** on initiation.[50,76,77] Additionally, tight complexation of **DMP** with **HFIP** may also prohibit ion-pairing of the reduced form with radical cations, leading to enhanced reactivity.[78] SET from anethole to **DMP** is computed as endergonic, as reflected by the overall negative electrochemical cell potential. The weakly oxidising iodinated reagent is employed to ensure that only a small amount of radical cation is produced *in situ* to avoid dimerisation and further oxidation to dications.[50,79,80]

2.2 Reactivity and selectivity between *trans*-anethole and *trans*-β-methylstyrene (P1)

For the reaction between *trans*-anethole **1a** and *trans*-β-methylstyrene **1b** (reaction P1) as shown in Scheme 2(a)(i), electron-rich alkene **1a** is preferentially oxidised by **DMP** *via* SET to give distonic radical cation $[\mathbf{1a}]^{\bullet+}$, which adds to the neutral alkene partner **1b** that is present in excess. Consistent with Wiest's earlier studies with B3LYP, no concerted 4-membered TS could be found on the M06-2X potential energy surface (PES). For the stepwise mechanism, both head-to-head and head-to-tail cyclobutanes are possible. In addition, *syn*- and *anti*-adducts can be formed depending on the orientation of the reacting alkenes when they approach each other. The Gibbs energy profile for both reaction pathways is given in Fig. 2. Possible conformations of the TSs were explored systematically (Fig. S2†) and the lowest energy conformers are presented here. The turnover-frequency determining transition state (TDTS) along the entire PES occurs during the first C–C bond forming step. The head-to-head TSs (**ts1** and **ts1′**) are kinetically more favourable, with a lower activation barrier than the head-to-tail TSs (**ts1-g1** and **ts1-g2**), by at least 4.7 kcal mol^{-1} (a selectivity of 410 : 1, using transition state theory), although the neutral, closed-shell cyclobutyl ring products lie closer in energy (within 1.1 kcal mol^{-1} of the observed product **int3n**, Fig. 2). For the head-to-head products, the *anti*-adduct **int3n** is favoured over the *syn*-adduct **int3′n** both kinetically (by 1.1 kcal mol^{-1}) and thermodynamically (by 2.1 kcal mol^{-1}). Although oxidation of the hypervalent iodine catalyst ($\mathbf{DMP}^{\bullet-}$) is easier than neutral *trans*-anethole, the reduction of radical cationic intermediates to the neutral, closed-shell cyclobutanes is more likely to involve anethole, present in larger amounts than the initiator. Additionally, cyclic voltammetry studies show irreversible reduction of the hypervalent iodine species taking place.[50] With this in mind, our computed energy profile uses *trans*-anethole as the reductant to complete the catalytic cycle.

The spin density in radical cation $[\mathbf{1a}]^{\bullet+}$ is predominantly localised on the β-carbon (Fig. 2 box). The benzylic carbocation is additionally stabilised by the *p*-methoxy lone pair. C–C bond formation occurs first at the β-carbon of both styrene partners (**ts1** and **ts1′**, Fig. S3†). This head-to-head combination forms an intermediate in which the positive charge and unpaired electron are stabilised at the two benzylic positions of **int2**. There is one benzylic position available for head-to-tail attack (**ts1-g1** and **ts1-g2**, Fig. S3†). Thus, the head-to-head TSs have much lower activation barriers (by more than 4.7 kcal mol^{-1}). The regioselectivity (head-to-head *vs.* head-to-tail) is kinetically controlled, as this first step is irreversible. Additionally, the ring-closed head-to-tail products **int3n-g1** and **int3n-g2** are close in energy to **int3n** but they are not observed, further supporting the absence of any interconversion of these products due to any reversibility of C–C formation. The electron transfer (ET) barrier for the reduction of the radical cationic products to their neutral form can be estimated using Marcus-Hush (MH) theory.[81–84] It was found that these barriers (on the order of 1–3 kcal mol^{-1}) are much smaller than any bond-forming barriers in the PES (ESI section 5†). Care should be noted, however, that the use of static, single-particle, DFT calculation in ET barrier estimation could possibly neglect effects of other electrons on the transfer.[85] The assumption of linear solvent response and the same curvature of reactant and product PESs could further introduce errors in our MH estimate.[86,87] Nevertheless, ET barriers on the order of 1–3 kcal mol^{-1} have been observed experimentally.[88–90] This suggests that this product-forming SET step is not overall rate-limiting. The reverse of this elementary step, oxidation of the cyclic products by the anethole radical cation, has an estimated (MH) barrier of about 14 kcal mol^{-1}. This is comparable to the barrier of the TDTS (Fig. 2) and suggests that this electron transfer can occur reversibly. This has stereochemical implications, since the overall barrier for cycloreversion (*via* **ts1′** from **int3′n**) of the minor diastereomer is 19.5 kcal mol^{-1} in **HFIP** (22.8 kcal mol^{-1} in MeCN). This permits equilibration to form the thermodynamically more favourable *all-trans* diastereomer at 40 °C. At lower temperatures (*e.g.* −35 °C) the diastereoselectivity is predicted to be lower, consistent with Bauld's experimental results (Scheme 2(b)).

To further understand the steric and electronic factors influencing the head-to-head *vs.* head-to-tail regioselectivity, we applied the distortion-interaction[91,92]/activation strain (DI–AS) model[92–96] to the TSs for the formation of first C–C bond for the present reaction (Fig. 3). As we can see, although the head-to-tail TSs have later transition states, evidenced by their shorter C–C bond in the TSs, the energetic penalty to distort the reacting molecules as they come together in the TSs, *i.e.*, the activation strain or the distortion energy (in blue), for all 4 TSs are similar; the head-to-tail TSs are disfavoured due to their less favourable interaction energies (in green) than the head-to-head TSs. Comparing the selectivity of **ts1** over **ts1′**, the distortion energies are identical whereas **ts1** has slightly more favourable interactions. The non-covalent interaction (NCI) plots in these TSs (Fig. 5) suggests that **ts1** benefits from favourable π–π stacking interaction (slightly staggered aryl rings) thus making it more favourable than **ts1′** having no such stacking interactions. This π–π stacking interaction is also observed in **ts6′** (but not **ts6**) (Fig. 5) such that the *syn*-addition **ts6′** has a lower activation

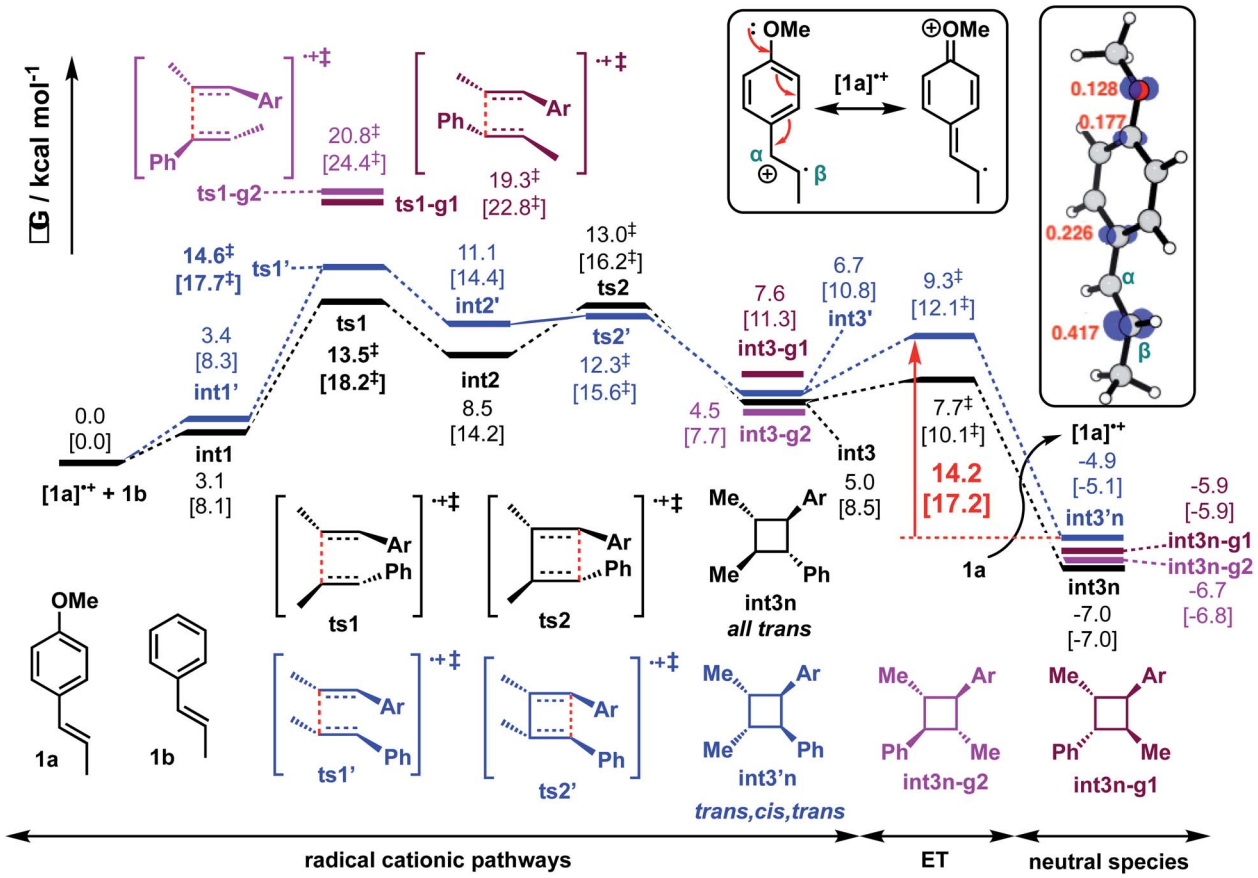

Fig. 2 Gibbs energy profile for reaction between *trans*-anethole and *trans*-β-methylstyrene computed at SMD(solvent)-M06-2X/def2-TZVPP//M06-2X/6-31G(d) level of theory. The values in **HFIP** are given together with values in MeCN in square brackets. ET = electron transfer barrier heights estimated using Marcus-Hush theory at an intermolecular separation of 3 Å (see ESI† for details). Spin density plots (at an isovalue of 0.02 a.u.) and the Mulliken spin density values of radical cationic *trans*-anethole is also shown.

barrier than the *anti*-addition **ts6** (activation strain model, Fig. S15†) (*vide infra*).

We further applied the method of energy decomposition analysis (with the ALMO-EDA method),[97–99] as applied in other similar systems,[94,96,100–102] to break down the contributions to the interaction energy between the reacting fragments into the repulsive exchange energy due to Pauli's principle, E_{Pauli}, the (semi-)classical electrostatic interaction energy between the charge densities of the fragments, E_{elec}, the orbital interaction energies between the fragments as the TS occurs, E_{orb}, and the dispersion energy between the fragments E_{disp}. Comparing the EDA between the major, *anti*-adduct *via* **ts1** to other TSs (Fig. S9–S11†) in pathway P1, we see that despite having larger Pauli repulsion, the much lower interaction energy in **ts1** is due to its much favourable dispersion (in agreement with NCI results) and electrostatic energies (not picked up by NCI analysis), although the orbital interaction energy is similar. In the comparison between **ts1** and **ts1′** for example, favourable non-covalent interactions stabilising **ts1** gains further support from the ALMO-EDA analysis (Fig. 4), which shows that the intermolecular dispersion energy is more stabilising for **ts1** than for **ts1′** along the reaction coordinate (green). There is in addition to a preferential electrostatic stabilisation (blue) in **ts1**. However, little difference in the orbital contribution (red) to the interaction energy is seen in both **ts1** and **ts1′**, since they have the same regiochemistry and bond formation occurs between the same pair of atoms. In the comparison of **ts1** with other regioisomeric transition structures (*e.g.*, **ts1** *vs.* **ts1-g1**, Fig. S10†), we see the additional contribution of the intermolecular orbital interaction energy (red) in favouring **ts1** along the reaction coordinate. The orbital preference for the major regioisomer can be understood from FMO-based arguments. The neutral alkene preferentially reacts with a cationic reagent at the β-position since this site has the larger HOMO coefficient. The radical cationic alkene reacts preferentially at the β-position since this is the site with higher spin density and greater SOMO coefficient.

Gibbs energies for all radical cationic intermediates in the reaction are preferentially stabilised in **HFIP** solvent than in MeCN solvent (by 3.2 to 5.7 kcal mol^{-1}), indicating the former solvent's ability in stabilising the charged intermediates;[50,76,77] the energies for the neutral species (**int3n**, **int3′n**, **int3n-g1** and **int3n-g2**), on the other hand, do not significantly differ in either solvent system (within 0.2 kcal mol^{-1}). This is not the result of bulk electrostatics, since it is MeCN that has a higher dielectric constant than **HFIP** (ε = 38.8 *vs.* 16.7). Rather, differences captured by parameters used by the SMD solvation model[103] relate to a greater Abraham's

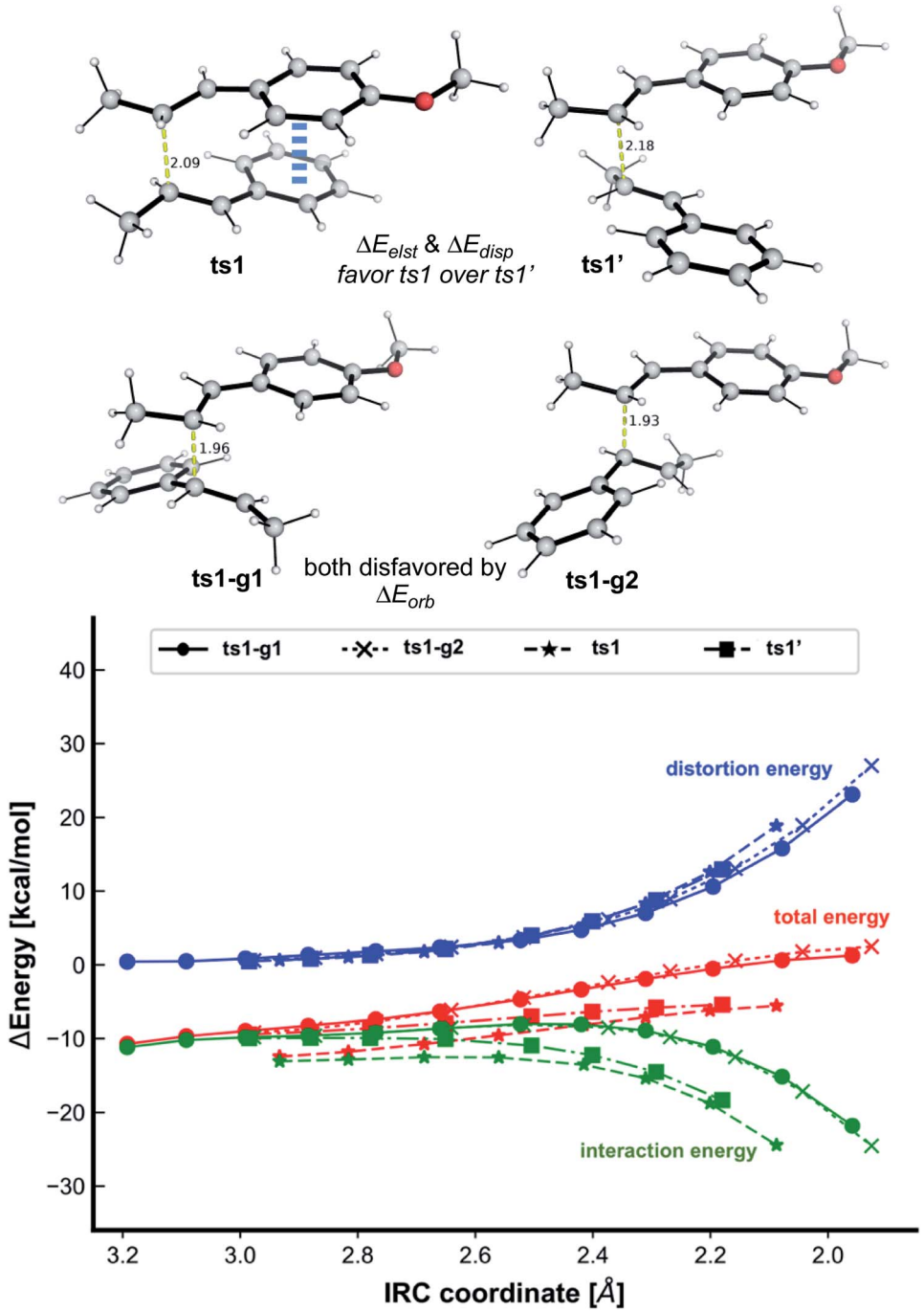

Fig. 3 The activation strain or distortion-interaction analyses applied to transition structures for both head-to-head (**ts1** and **ts1′**) and head-to-tail (**ts1-g1** and **ts1-g2**) first C–C bond formation TSs (optimised structures given). All energies are calculated at UM062X/def2TZVPP//UM062X/6-31G(d) and used without any further corrections.

hydrogen bond acidity of **HFIP** than MeCN (1.96 *vs.* 0.07) and electronegative halogenicity (0.6 *vs.* 0.0), which reflect the difference in Gibbs energy change associated with cavitation, dispersion and solvent structure for these two solvents.[104–106]

2.3 Reactivity and selectivity between *trans*-anethole and *cis*-β-methylstyrene (P2)

We similarly investigated the SET hole-catalysed reaction between *trans*-anethole **1a** and *cis*-β-methylstyrene **2b** (reaction P2) as shown in Scheme 2(a)(ii). From the calculated redox potentials for these substrates in Table 1, *trans*-anethole **1a** will be oxidised preferentially to *cis*-β-methylstyrene **2b** by the hypervalent iodine reagent in the fluorinated solvent. The Gibbs energy profile for both head-to-head and head-to-tail cyclobutanation is shown in Fig. 5 (See Fig. S12† for all possible conformations). The *syn*-addition (blue pathway) has the lowest activation barrier, at 15.1 kcal mol^{-1}, with **ts7′** (the second C–C bond formation) as the overall TDTS. The *anti*-addition (black

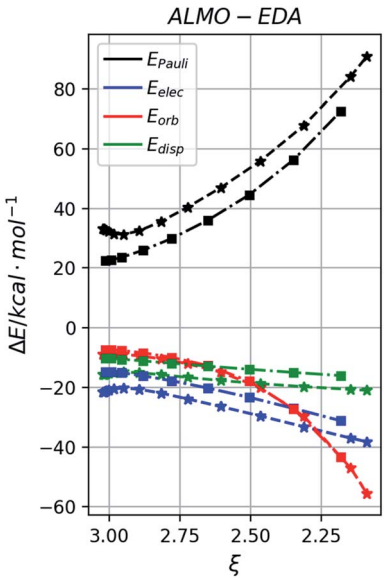

Fig. 4 Comparison of the absolutely-localized molecular orbitals energy decomposition analysis (ALMO-EDA) for **ts1** (star marker) and **ts1′** (square marker) in reaction P1.

pathway) has **ts6** (first C–C bond formation) as the overall TDTS, at 17.1 kcal mol^{-1}. Comparing the first C–C bond formation TSs **ts6** and **ts6′**, the *syn*-addition **ts6′** is lower than the *anti*-addition **ts6**, by 3.3 kcal mol^{-1}. The TS **ts6′** benefits from π–π stacking interaction that is absent in **ts6** as evidenced by NCI plots in Fig. 6. This is similar to pathway P1, where the *anti*-addition **ts1** is lower in activation barrier than *syn*-addition **ts1′**, where π–π stacking interaction is also observed for **ts1**, as discussed previously.

Activation barriers for head-to-head additions are again lower due to the preferential location of the radical cation at the two benzylic α-positions (spin density plots, Fig. S13†). DI–AS analysis of the first C–C bond formation TSs shows again that the interaction energy is more favourable in head-to-head isomers than in head-to-tail isomers whereas the distortion energies are similar in all cases, as in pathway P1. ALMO-EDA comparison between the major *syn*-addition pathway (*via* **ts6′**) and other pathways (Fig. S20–S22†) suggests that dispersion and electrostatic interactions contributes favourably to **ts6′** selectivity despite its higher Pauli repulsion, as observed for **ts1** in reaction P1. We note that no *trans*,*trans*,*cis* product, **int8n**, is observed experimentally. Product **int8′n** is kinetically favoured by 2.0 kcal mol^{-1} and thermodynamically favoured by 1.2 kcal mol^{-1} than product **int8n**.

The Gibbs energy profile in Fig. 5 explains the selectivity in favour of the formation of *trans*,*cis*,*cis* cyclobutane **int8′n** arising from *syn*-addition. Experimentally, in addition to this product, the *all-trans* cyclobutane **int3n** is also formed. The diastereomeric ratio of **int8′n** : **int3n** is 4 : 1 (Scheme 2(a)(ii)). The cycloadduct **int3n** cannot be formed directly from the starting materials in the present transformation; two possibilities could occur to yield **int3n**: either *cis*-β-methylstyrene undergoes isomerisation to give *trans*-β-methylstyrene before formal [2 + 2] cycloaddition, or the intermediates after first C–C bond formation undergo rotation before the second C–C bond formation/cyclisation to yield product **int3n**. The isomerisation of neutral *cis*-β-methyl-styrene to its *trans*-form cannot be

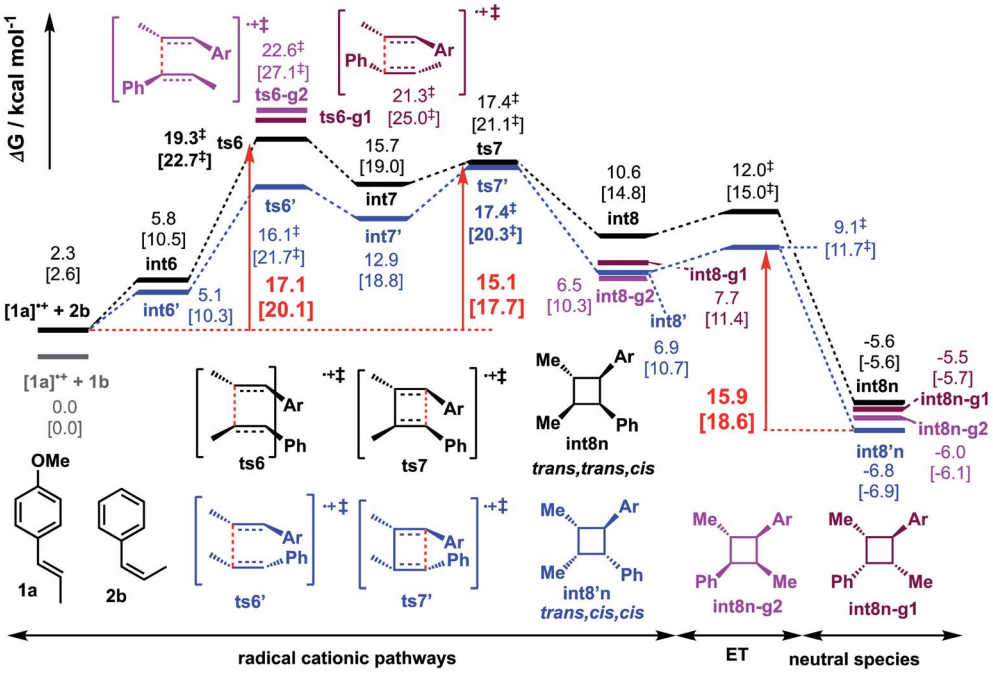

Fig. 5 Gibbs energy profile for reaction between *trans*-anethole and *cis*-β-methylstyrene computed at SMD(solvent)-M06-2X/def2-TZVPP//M06-2X/6-31G(d) level of theory. Same energy zero is used as previously. ET = electron transfer barrier heights estimated using Marcus-Hush theory at an intermolecular separation of 3 Å (see ESI† for details). The values in HFIP are given together with values in MeCN in square brackets.

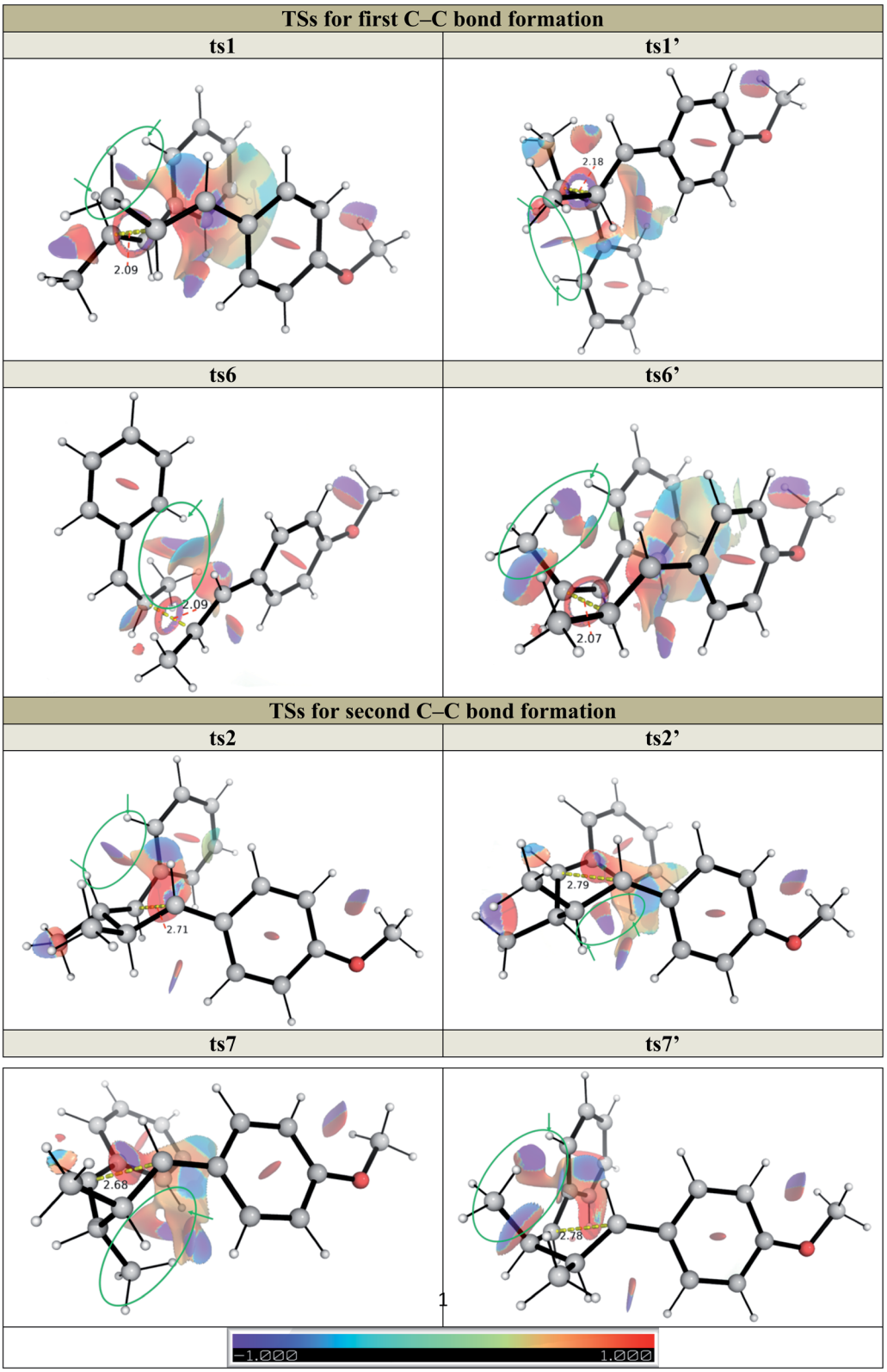

Fig. 6 Non-covalent interaction (NCI) plots for key TSs in pathways P1 and P2 at gradient isosurface value of $s = 0.5$ a.u.

achieved thermally at the reaction temperature, requiring *ca.* 60 kcal mol^{-1}.[107,108] Alternatively, *cis*-to-*trans* isomerisation of β-methylstyrene *via* hole-catalysed rotation can be achieved more readily than in the neutral counterpart,[109] however, the higher redox potential of *cis*-β-methylstyrene **2b** than *trans*-anethole **1a** (521 mV difference in **HFIP**, Table 1) implies the latter would

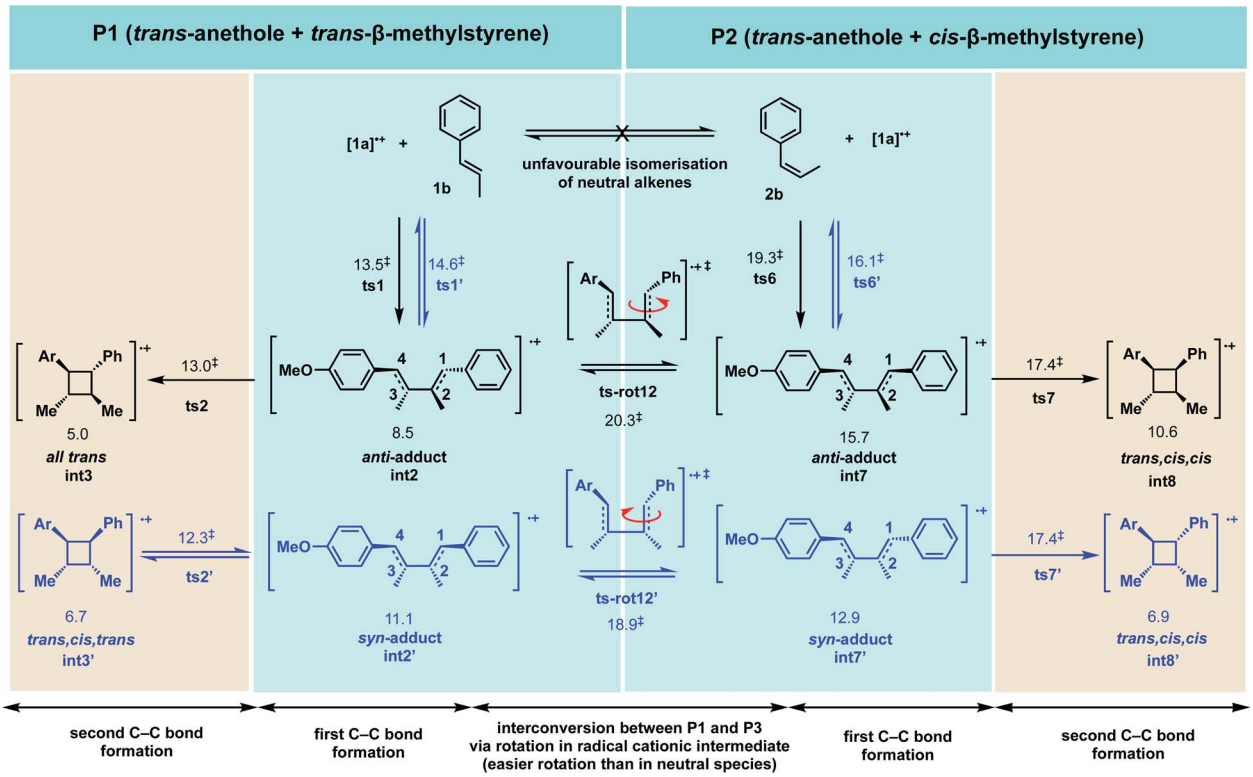

Scheme 4 Interconversion between reaction pathways involving *trans*-anethole and *trans*-β-methylstyrene (P1) and *trans*-anethole and *cis*-β-methylstyrene (P2) *via* rotations in the radical cationic intermediates. Gibbs energies in HFIP solvents are given in kcal mol^{-1}.

preferentially form a radical cation first (a preference of *ca.* 12 kcal mol^{-1}), which subsequently attacks the neutral *cis*-β-methylstyrene, present in excess. The 1 : 2 stoichiometric ratio of the two alkenes **1a** : **2b** (even though this increases slightly during the reaction as reactants are consumed) is not enough to outweigh the intrinsic difference in oxidation potentials such that we consider the possibility in the isomerisation of radical cationic *cis*-β-methylstyrene unlikely.

We therefore focused our attention on the rotation of the acyclic radical cation intermediates formed after the first step. Free rotation about C–C single bonds in radical cationic systems are known to be relatively facile;[57,86] these rotations can be more easily achieved in radical cationic species than in their neutral counterparts.[109] Scheme 4 shows the reactions between *trans*-anethole **1a** and either *trans*-β-methylstyrene **1b** (P1) or *cis*-β-methylstyrene **2b** (P2). These two reactions are interconvertible *via* a rotation about C1–C2 bond in the radical cationic intermediate following first C–C bond formation. In the reaction between [**1a**]$^{\bullet+}$ and **1b** for example (P1), at the intermediate **int2** after the first C–C bond formation, direct second C–C bond formation (**ts2**, 13.0 kcal mol^{-1}) has a much lower activation barrier than the rotational barrier to access pathways P2 (**ts-rot-12**, 20.3 kcal mol^{-1}), such that only **int3n** is formed as the sole product.

In the reaction between [**1a**]$^{\bullet+}$ and **2b** (P2), after the first reversible C–C bond formation, the intermediate **int7′** can undergo a direct second C–C bond formation **ts7′**, with an activation barrier of 17.4 kcal mol^{-1}. In this scenario, however, the rotational barrier is much more competitive (**ts-rot-12′**, 18.9 kcal mol^{-1}) to give **int2′**, allowing the reaction to access pathway P1. This intermediate **int2′** could form neutral cyclobutyl ring **int3′n** directly due to the low barriers for the second C–C bond formation and the electron transfer to reduce the radical cationic cyclobutyl **int3′**. This neutral cyclobutene **int3′n** could also be reduced back to its radical cationic **int3′** with a barrier of 14.2 kcal mol^{-1}, which is (slightly) lower than the overall TDTS **ts1′** at 14.6 kcal mol^{-1}. The cycloreversion[110,111] of **int3′** would give [**1a**]$^{\bullet+}$ and **1b**, which subsequently forms **int3n** as the thermodynamic product. In a way, we can think of the radical cationic species **int7′** as an intermediate for the conversion of *cis*-β-methylstyrene to *trans*-β-methylstyrene before further reaction to give the *all-trans* cyclobutane. Note that structures **int3n** and **int8′n** are almost isoenergetic and are favoured both kinetically (by 1.6–2.0 kcal mol^{-1}) and thermodynamically (by 1.2–2.1 kcal mol^{-1}) over **int3′n** and **int8n**. The activation barrier difference $\Delta\Delta G^{\ddagger}$ of 1.5 kcal mol^{-1} between second C–C bond formation/cyclisation (**ts7′**, 17.4 kcal mol^{-1}) and rotation (**ts-rot-12′**, 18.9 kcal mol^{-1}) gives a selectivity ratio of 6.8 : 1 under kinetic control; this is close to the experimentally observed ratio of 4 : 1. The exact ratio is likely influenced by dynamical effects in such radical cationic intermediates, shown in a quantum classical dynamics study of radical cationic Diels–Alder cycloaddition.[112]

Comparing reactions P1 and P2, we note that for both the first and second C–C bond formations, the TSs for P1, where both alkenes involved have *trans*-geometry, are lower in

activation barrier than the TSs for P2, where one of the alkenes has *cis*-geometry whereas the other *trans*-geometry. From Fig. 6 (and Fig. S2 and S12†), the bond lengths in TSs for first (**ts1**, **ts1′**, **ts6** and **ts6′**) and second (**ts2**, **ts2′**, **ts7** and **ts7′**) C–C bond formations are similar for both pathways P1 and P2 (to within 0.1 Å). The TSs in P1 (**ts1** and **ts1′** for first C–C bond formation and **ts2** and **ts2′** for second C–C bond formation), however, all have lower activation barriers than the corresponding TSs in P2 (**ts6** and **ts6′** for first C–C bond formation and **ts7** and **ts7′** for second C–C bond formation), since there is less steric clashes between the O–H atom on the phenyl ring and the H atom on β-carbon of *trans*-β-methylstyrene in P1 than between the O–H atom on the phenyl ring and the methyl group on the β-carbon *cis*-β-methylstyrene in P2, giving greater reactivity in reaction P1 than reaction P2.

3. Conclusions

We have studied the heterodimerisation of styrenes promoted by hypervalent iodine oxidants with DFT calculations. The homodimerisation of anethole is computed to occur around 56 times faster than heterodimerisation ($\Delta\Delta G^{\ddagger} = 2.5$ kcal mol^{-1}). Experimentally, low concentrations of anethole are necessary to avoid homodimerisation. Anethole is added (dropwise) to a solution of an otherwise unreactive alkene in excess (2 equiv.) to ensure heterodimerisation occurs. Computed reduction potentials with implicit and explicit models of solvation indicate that **HFIP** solvation creates a more powerful oxidant by stabilising the radical anionic form of the hypervalent iodine species, forming strong intermolecular hydrogen bonds. The regioselectivity for head-to-head dimerisation results from a kinetic preference in the first C–C bond forming step. In the heterodimerisation of two *trans*-styrenes (reaction P1) complete stereoretention is observed. The *all-trans* diastereomer is favoured kinetically over the *trans–cis–trans* form in the first step, and this preference is further reinforced by the greater thermodynamic stability of the *all-trans* product and the potential for overall reversibility at ambient temperatures and above. TSs that result in the loss of alkene stereochemistry by an exocyclic rotation in the acylic radical cation intermediates lie more than 4 kcal mol^{-1} above all C–C bond forming TSs and do not play a role for these substrates. In contrast, C–C forming TSs in the reaction between a *trans*- and a *cis*-alkene (reaction P2) lie higher in energy, such that rotation is now competitive with ring-closure. This results in the formation of products that are normally formed from the reaction of two alkenes of *trans*-geometry. In addition, *anti*-addition (giving *trans*-geometry across the first C–C bond formation) is favoured when the reacting alkenes are both of *trans*-geometry whereas *syn*-addition (*cis*-geometry across the first C–C bond formation) is favoured when one of the reacting alkenes is of *cis*-geometry. These calculations agree with the stereochemical results of recent studies with hypervalent iodine oxidants, and with previous studies using amininum oxidants.

We have shown that the radical cation mediated hole-catalysed cycloaddition is predominantly influenced by electronic factors and is under both kinetic and thermodynamic controls. The regioselectivity for head-to-head over head-to-tail isomer formations is under kinetic control, as both these neutral 4-membered rings have rather close energies. For the head-to-head isomers (*syn- vs. anti*-adducts), although the major isomer is favoured both kinetically and thermodynamically, the product selectivity is controlled by thermodynamics of the neutral products since the experimentally observed product distribution agrees better with the thermodynamic energetic differences rather than the kinetic activation barrier differences.

Alkene heterodimerisation with "hole catalysis" is intrinsically challenging since the more electron-rich reagent is both easier to oxidize and more reactive towards the radical cation once it has been formed. We predict that the homodimerisation pathway for *trans*-anethole is kinetically favoured by 2.5 kcal mol^{-1} over the heterodimerisation with β-methylstyrene where the concentrations of the two alkenes are identical. Practical solutions to this challenge have thus far focused on increasing the amount of the less electron-rich alkene and adding the more electron-rich component dropwise. Based on our analysis of the competing transition structures, and in particular those features that favour heterodimerisation **ts1**, we propose enhancing attractive dispersive and electrostatic interactions as an alternative way to increase the likelihood of heterodimerisation. For example, we expect that incorporation of larger π-systems or aromatic substituents known to provide greater dispersive interactions into the less easily oxidised alkene will stabilise heterodimerisation **ts1**. Additionally, through-space electrostatic interactions could also be optimised for the less electron-rich component by the introduction of polar functional groups that are not in direct conjugation with the alkene. Such groups could then stabilise the heterodimerisation pathway without a large change in oxidation potential to this component. Since dispersive and electrostatic contributions also stabilise **ts1** over diasteromeric pathways, tuning these interactions could also be used to ensure high levels of diastereoselectivity. The understanding of this mechanism opens up possibilities of experimentally controlling the chemoselectivity, regioselectivity and stereoselectivity in oxidant-promoted SET hole-catalysed heterodimerisation of electron-rich alkenes in accessing complex, tetra-substituted cyclobutyl rings. Using computational calculations of redox potentials of different alkenes and understanding their inherent steric and electronic properties, we envision that intermolecular heterodimerisation of different alkenes can be efficiently controlled, with precise chemical selectivity, to efficiently access tetra-substituted cyclobutanes.

Conflicts of interest

There are no conflicts to declare.

Acknowledgements

Funding from the Agency for Science, Technology and Research (A*STAR), Singapore (X. Z.) is gratefully acknowledged. X. Z. and R. S. P. acknowledge the EPSRC Centre for Doctoral Training in

Theory and Modelling in Chemical Sciences (EP/L015722/1) and the use of Dirac cluster. X. Z. thanks Dr Maria Koiyoni for her help with **HFIP** solvent parametrisation. R. S. P. acknowledges computational resources from the RMACC Summit supercomputer supported by the National Science Foundation (ACI-1532235 and ACI-1532236), the University of Colorado Boulder and Colorado State University, and the Extreme Science and Engineering Discovery Environment (XSEDE) through allocation TG-CHE180056. XSEDE is supported by the National Science Foundation (ACI-1548562). We thank Prof. Aqeel Hussain for sharing information with us.[113]

References

1 V. M. Dembitsky, Bioactive Cyclobutane-Containing Alkaloids, *J. Nat. Med.*, 2008, **62**(1), 1–33.
2 A. Sergeiko, V. V. Poroikov, L. O. Hanus and V. M. Dembitsky, Cyclobutane-Containing Alkaloids: Origin, Synthesis, and Biological Activities, *Open Med. Chem. J.*, 2008, **2**(1), 26–37.
3 J. C. Namyslo and D. E. Kaufmann, The Application of Cyclobutane Derivatives in Organic Synthesis, *Chem. Rev.*, 2003, **103**(4), 1485–1538.
4 T. Seiser, T. Saget, D. N. Tran and N. Cramer, Cyclobutanes in Catalysis, *Angew. Chem., Int. Ed.*, 2011, **50**(34), 7740–7752.
5 E. V. Anslyn and D. A. Dougherty, Chapter 2: Strain and Stability, in *Modern Physical Organic Chemistry*, University Science, Sausalito, CA, 2006, pp. 100–109.
6 C. Liebermann, Ueber Polythymochinon, *Ber. Dtsch. Chem. Ges.*, 1877, **10**(2), 2177–2179.
7 S. Farid and S. E. Shealer, Radical Cations: Photochemical and Ferric Ion-Induced Formation and Reactions of Indene Radical Cation, *J. Chem. Soc., Chem. Commun.*, 1973, **0**(18), 677–678.
8 S. Kuwata, Y. Shigemitsu and Y. Odaira, Photosensitized Cyclodimerization of Phenyl Vinyl Ether, *J. Chem. Soc., Chem. Commun.*, 1972, **0**(1), 2.
9 R. A. Caldwell, K. Mizuno, P. E. Hansen, L. P. Vo, M. Frentrup and C. D. Ho, Photochemistry of the Phenanthrene-Stilbene System. Cycloaddition and Singlet-Sensitized Isomerization, *J. Am. Chem. Soc.*, 1981, **103**(24), 7263–7269.
10 T. Bach and J. P. Hehn, Photochemical Reactions as Key Steps in Natural Product Synthesis, *Angew. Chem., Int. Ed.*, 2011, **50**(5), 1000–1045.
11 Y. J. Hong and D. J. Tantillo, How Cyclobutanes Are Assembled in Nature-Insights from Quantum Chemistry, *Chem. Soc. Rev.*, 2014, **43**(14), 5042–5050.
12 S. Poplata, A. Tröster, Y. Q. Zou and T. Bach, Recent Advances in the Synthesis of Cyclobutanes by Olefin [2 +2] Photocycloaddition Reactions, *Chem. Rev.*, 2016, **116**(17), 9748–9815.
13 I. Colomer, R. Coura Barcelos and T. J. Donohoe, Catalytic Hypervalent Iodine Promoters Lead to Styrene Dimerization and the Formation of Tri- and Tetrasubstituted Cyclobutanes, *Angew. Chem., Int. Ed.*, 2016, **55**(15), 4748–4752.
14 Ł. Albrecht, G. Dickmeiss, F. C. Acosta, C. Rodríguez-Escrich, R. L. Davis and K. A. Jørgensen, Asymmetric Organocatalytic Formal [2 + 2]-Cycloadditions *via* Bifunctional H-Bond Directing Dienamine Catalysis, *J. Am. Chem. Soc.*, 2012, **134**(5), 2543–2546.
15 A. J. Nielsen, H. A. Jenkins and J. McNulty, Asymmetric Organocatalytic Stepwise [2 + 2] Entry to Tetra-Substituted Heterodimeric and Homochiral Cyclobutanes, *Chem. - Eur. J.*, 2016, **22**(27), 9111–9115.
16 C. K. Prier, D. A. Rankic and D. W. C. MacMillan, Visible Light Photoredox Catalysis with Transition Metal Complexes: Applications in Organic Synthesis, *Chem. Rev.*, 2013, **113**(7), 5322–5363.
17 M. Lautens, W. Klute and W. Tam, Transition Metal-Mediated Cycloaddition Reactions, *Chem. Rev.*, 1996, **96**(1), 49–92.
18 V. A. Schmidt, J. M. Hoyt, G. W. Margulieux and P. J. Chirik, Cobalt-Catalyzed [2π + 2π] Cycloadditions of Alkenes: Scope, Mechanism, and Elucidation of Electronic Structure of Catalytic Intermediates, *J. Am. Chem. Soc.*, 2015, **137**(24), 7903–7914.
19 K. Chiba, T. Miura, S. Kim, Y. Kitano and M. Tada, Electrocatalytic Intermolecular Olefin Cross-Coupling by Anodically Induced Formal [2 + 2] Cycloaddition between Enol Ethers and Alkenes, *J. Am. Chem. Soc.*, 2001, **123**(45), 11314–11315.
20 M. Arata, T. Miura and K. Chiba, Electrocatalytic Formal [2 + 2] Cycloaddition Reactions between Anodically Activated Enyloxy Benzene and Alkenes, *Org. Lett.*, 2007, **9**(21), 4347–4350.
21 T. Miura, S. Kim, Y. Kitano, M. Tada and K. Chiba, Electrochemical Enol Ether/Olefin Cross-Metathesis in a Lithium Perchlorate/Nitromethane Electrolyte Solution, *Angew. Chem., Int. Ed.*, 2006, **45**(9), 1461–1463.
22 K. Chiba and M. Tada, Diels–Alder Reaction of Quinones Generated *in situ* by Electrochemical Oxidation in Lithium Perchlorate-Nitromethane, *J. Chem. Soc., Chem. Commun.*, 1994, 2485–2486.
23 W. R. Gutekunst and P. S. Baran, Applications of C–H Functionalization Logic to Cyclobutane Synthesis, *J. Org. Chem.*, 2014, **79**(6), 2430–2452.
24 Q. F. Wu, X. B. Wang, P. X. Shen and J. Q. Yu, Enantioselective C–H Arylation and Vinylation of Cyclobutyl Carboxylic Amides, *ACS Catal.*, 2018, **8**(3), 2577–2581.
25 J.-L. Hu, L.-W. Feng, L. Wang, Z. Xie, Y. Tang and X. Li, Enantioselective Construction of Cyclobutanes: A New and Concise Approach to the Total Synthesis of (+)-Piperarborenine B, *J. Am. Chem. Soc.*, 2016, **138**(40), 13151–13154.
26 X. Yang, G. Shan, Z. Yang, G. Huang, G. Dong, C. Sheng and Y. Rao, One-Pot Synthesis of Quaternary Carbon Centered Cyclobutanes *via* Pd(II)-Catalyzed Cascade $C(sp^3)$–H Activations, *Chem. Commun.*, 2017, **53**(9), 1534–1537.
27 V. Mascitti and E. J. Corey, Total Synthesis of (±)-Pentacycloanammoxic Acid, *J. Am. Chem. Soc.*, 2004, **126**(48), 15664–15665.

28 P. Lu and T. Bach, Total Synthesis of (+)-Lactiflorin by an Intramolecular [2 + 2] Photocycloaddition, *Angew. Chem., Int. Ed.*, 2012, **51**(5), 1261–1264.
29 P. Zhang, Y. Wang, R. Bao, T. Luo, Z. Yang and Y. Tang, Enantioselective Biomimetic Total Syntheses of Katsumadain and Katsumadain C, *Org. Lett.*, 2012, **14**(1), 162–165.
30 S. E. Reisman, J. M. Ready, A. Hasuoka, C. J. Smith and J. L. Wood, Total Synthesis of (±)-Welwitindolinone A Isonitrile, *J. Am. Chem. Soc.*, 2006, **128**(5), 1448–1449.
31 F. D. Piaz, A. Vassallo, A. Temraz, R. Cotugno, M. A. Belisario, G. Bifulco, M. G. Chini, C. Pisano, N. De Tommasi and A. Braca, A Chemical-Biological Study Reveals C9-Type Iridoids as Novel Heat Shock Protein 90 (Hsp90) Inhibitors, *J. Med. Chem.*, 2013, **56**(4), 1583–1595.
32 L. Eberson, Catalysis by Electron Transfer in Organic Chemistry, *J. Mol. Catal.*, 1983, **20**(1), 27–52.
33 M. A. Ischay and T. P. Yoon, Accessing the Synthetic Chemistry of Radical Ions, *Eur. J. Org. Chem.*, 2012, **2012**(18), 3359–3372.
34 S. Lin, S. D. Lies, C. S. Gravatt and T. P. Yoon, Radical Cation Cycloadditions Using Cleavable Redox Auxiliaries, *Org. Lett.*, 2017, **19**(2), 368–371.
35 Y. Yamaguchi, Y. Okada and K. Chiba, Understanding the Reactivity of Enol Ether Radical Cations: Investigation of Anodic Four-Membered Carbon Ring Formation, *J. Org. Chem.*, 2013, **78**(6), 2626–2638.
36 O. Cortezano-Arellano, L. Quintero and F. Sartillo-Piscil, Total Synthesis of Cephalosporolide E *via* a Tandem Radical/Polar Crossover Reaction. The Use of the Radical Cations under Nonoxidative Conditions in Total Synthesis, *J. Org. Chem.*, 2015, **80**(5), 2601–2608.
37 M. S. Alehashem, C. G. Lim and N. F. Thomas, The Radical Cation Mediated Cleavage of Catharanthine Leading to the Vinblastine Type Alkaloids: Implications for Total Synthesis and Drug Design, *RSC Adv.*, 2016, **6**(22), 18002–18025.
38 F. A. Bell, R. A. Crellin, H. Fujii and A. Ledwith, Cation-Radicals: Metal-Catalysed Cyclodimerisation of Aromatic Enamines, *J. Chem. Soc. D*, 1969, **6**, 251–252.
39 L.-Q. Q. Liu, D.-Q. Q. Sun and J.-K. K. Yang, Efficient Additives to Improve the Catalytic Effects of Ferric(III) Chloride on the Reaction of N-Vinylcarbazole: Hydroquinone for Methanolysis, Hydrogen Peroxide for Cyclobutanation Respectively, *J. Phys. Org. Chem.*, 2012, **25**(4), 272–277.
40 Y. Yu, Y. Fu and F. Zhong, Benign Catalysis with Iron: Facile Assembly of Cyclobutanes and Cyclohexenes: *Via* Intermolecular Radical Cation Cycloadditions, *Green Chem.*, 2018, **20**(8), 1743–1747.
41 M. Riener and D. A. Nicewicz, Synthesis of Cyclobutane Lignans *via* an Organic Single Electron Oxidant-Electron Relay System, *Chem. Sci.*, 2013, **4**(6), 2625–2629.
42 Z. Lu and T. P. Yoon, Visible Light Photocatalysis of [2 + 2] Styrene Cycloadditions by Energy Transfer, *Angew. Chem., Int. Ed.*, 2012, **51**(41), 10329–10332.
43 J. Du and T. P. Yoon, Crossed Intermolecular [2 + 2] Cycloadditions of Acyclic Enones *via* Visible Light Photocatalysis, *J. Am. Chem. Soc.*, 2009, **131**(41), 14604–14605.
44 M. A. Ischay, M. S. Ament and T. P. Yoon, Crossed Intermolecular [2 + 2] Cycloaddition of Styrenes by Visible Light Photocatalysis, *Chem. Sci.*, 2012, **3**(9), 2807–2811.
45 A. E. Hurtley, Z. Lu and T. P. Yoon, Cycloaddition of 1,3-Dienes by Visible Light Photocatalysis, *Angew. Chem., Int. Ed.*, 2014, **53**(34), 8991–8994.
46 N. L. Bauld and R. Pabon, Cation Radical Catalyzed Olefin Cyclodimerization, *J. Am. Chem. Soc.*, 1983, **105**(3), 633–634.
47 P. G. Gassman and D. A. Singleton, Distinction between Aminium Cation Radical and Protic Acid Catalyzed Diels-Alder Reactions, *J. Am. Chem. Soc.*, 1984, **106**(25), 7993–7994.
48 D. W. Reynolds, K. T. Lorenz, H. S. Chiou, D. J. Bellville, R. A. Pabon and N. L. Bauld, Mechanistic Diagnosis of Aminium Salt Initiated Diels-Alder Cycloadditions in the Diene/Diene Format, *J. Am. Chem. Soc.*, 1987, **109**(16), 4960–4968.
49 N. L. Bauld, J. Yang and D. Gao, Diels–Alder Cycloadditions of the *N*-Vinylcarbazole Radical Cation, *J. Chem. Soc., Perkin Trans. 2*, 2000, (2), 207–210.
50 I. Colomer, C. Batchelor-Mcauley, B. Odell, T. J. Donohoe and R. G. Compton, Hydrogen Bonding to Hexafluoroisopropanol Controls the Oxidative Strength of Hypervalent Iodine Reagents, *J. Am. Chem. Soc.*, 2016, **138**(28), 8855–8861.
51 A. Ledwith, Cation Radicals in Electron Transfer Reactions, *Acc. Chem. Res.*, 1972, **5**(4), 133–139.
52 S. L. Mattes and S. Farid, Photooxygenation *via* Electron Transfer. 1,1-Dimethylindene, *J. Am. Chem. Soc.*, 1982, **104**(5), 1454–1456.
53 S. L. Mattes and S. Farid, Photosensitized Electron-Transfer Reactions. Interception of the Geminate Radical Ion Pair, *J. Am. Chem. Soc.*, 1983, **105**(5), 1386–1387.
54 S. L. Mattes and S. Farid, Photochemical Electron-Transfer Reactions of 1,1-Diarylethylenes, *J. Am. Chem. Soc.*, 1986, **108**(23), 7356–7361.
55 D. W. Reynolds, B. Harirchian, H.-S. Chiou, B. K. Marsh and N. L. Bauld, The Cation Radical Vinylcyclobutane Rearrangement, *J. Phys. Org. Chem.*, 1989, **2**(1), 57–88.
56 N. P. Schepp and L. J. Johnston, Nanosecond and Picosecond Dynamics of the Radical Cation Mediated Dimerization of 4-Methoxystyrene, *J. Am. Chem. Soc.*, 1994, **116**(15), 6895–6903.
57 L. J. Johnston and N. P. Schepp, in *Advances in Electron Transfer*, ed. P. S. Mariano, JAI Press, New York, 1996, vol. 6, pp. 41–102.
58 L. L. O'Neil and O. Wiest, Acyclic or Long-Bond Intermediate in the Electron-Transfer-Catalyzed Dimerization of 4-Methoxystyrene, *J. Org. Chem.*, 2006, **71**(23), 8926–8933.
59 C. A. Marquez, H. Wang, F. Fabbretti and J. O. Metzger, Electron-Transfer-Catalyzed Dimerization of Trans-Anethole: Detection of the Distonic Tetramethylene Radical Cation Intermediate by Extractive Electrospray

Ionization Mass Spectrometry, *J. Am. Chem. Soc.*, 2008, **130**(51), 17208–17209.

60 C. Guo, L. Cui, B. Chen, J. Yuan and Z. Tian, A Theoretical Study on the Stereoconvergency of the Intramolecular Radical Cation [2 + 2] Cycloadditions of Bis(Styrenes), *RSC Adv.*, 2012, **2**(26), 9932–9937.

61 Y. Li, C. Guo and B.-Z. Chen, A Theoretical Study on Intermolecular [2 + 2] Radical Cation Cycloaddition Reactions and the Competition between Concerted and Stepwise Mechanisms, *Comput. Theor. Chem.*, 2016, **1078**, 163–172.

62 M. H. Baik and R. A. Friesner, Computing Redox Potentials in Solution: Density Functional Theory as a Tool for Rational Design of Redox Agents, *J. Phys. Chem. A*, 2002, **106**(32), 7407–7412.

63 P. Winget, C. J. Cramer and D. G. Truhlar, Computation of Equilibrium Oxidation and Reduction Potentials for Reversible and Dissociative Electron-Transfer Reactions in Solution, *Theor. Chem. Acc.*, 2004, **112**(4), 217–227.

64 Y. Fu, L. Liu, H.-Z. Yu, Y.-M. Wang and Q.-X. Guo, Quantum-Chemical Predictions of Absolute Standard Redox Potentials of Diverse Organic Molecules and Free Radicals in Acetonitrile, *J. Am. Chem. Soc.*, 2005, **127**(19), 7227–7234.

65 M. Schmidt Am Busch and E. W. Knapp, One-Electron Reduction Potential for Oxygen- and Sulfur-Centered Organic Radicals in Protic and Aprotic Solvents, *J. Am. Chem. Soc.*, 2005, **127**(45), 15730–15737.

66 P. Jaque, A. V. Marenich, C. J. Cramer and D. G. Truhlar, Computational Electrochemistry: The Aqueous $Ru^{3+}|Ru^{2+}$ Reduction Potential, *J. Phys. Chem. C*, 2007, **111**(15), 5783–5799.

67 A. S. Dutton, J. M. Fukuto and K. N. Houk, Theoretical Reduction Potentials for Nitrogen Oxides from CBS-QB3 Energetics and (C)PCM Solvation Calculations, *Inorg. Chem.*, 2005, **44**(11), 4024–4028.

68 J. L. Hodgson, M. Namazian, S. E. Bottle and M. L. Coote, One-Electron Oxidation and Reduction Potentials of Nitroxide Antioxidants: A Theoretical Study, *J. Phys. Chem. A*, 2007, **111**(51), 13595–13605.

69 L. E. Roy, E. Jakubikova, M. Graham Guthrie and E. R. Batista, Calculation of One-Electron Redox Potentials Revisited. Is It Possible to Calculate Accurate Potentials with Density Functional Methods?, *J. Phys. Chem. A*, 2009, **113**(24), 6745–6750.

70 G. Gryn'ova, J. M. Barakat, J. P. Blinco, S. E. Bottle and M. L. Coote, Computational Design of Cyclic Nitroxides as Efficient Redox Mediators for Dye-Sensitized Solar Cells, *Chem.–Eur. J.*, 2012, **18**(24), 7582–7593.

71 A. V. Marenich, A. Majumdar, M. Lenz, C. J. Cramer and D. G. Truhlar, Construction of Pourbaix Diagrams for Ruthenium-Based Water-Oxidation Catalysts by Density Functional Theory, *Angew. Chem., Int. Ed.*, 2012, **51**(51), 12810–12814.

72 B. T. Psciuk and H. B. Schlegel, Computational Prediction of One-Electron Reduction Potentials and Acid Dissociation Constants for Guanine Oxidation Intermediates and Products, *J. Phys. Chem. B*, 2013, **117**(32), 9518–9531.

73 J. Ho, Are Thermodynamic Cycles Necessary for Continuum Solvent Calculation of PK a s and Reduction Potentials?, *Phys. Chem. Chem. Phys.*, 2015, **17**(4), 2859–2868.

74 A. V. Marenich, J. Ho, M. L. Coote, C. J. Cramer and D. G. Truhlar, Computational Electrochemistry: Prediction of Liquid-Phase Reduction Potentials, *Phys. Chem. Chem. Phys.*, 2014, **16**(29), 15068–15106.

75 H. G. Roth, N. A. Romero, D. A. Nicewicz, H. G. Roth, N. A. Romero, D. A. Nicewicz, H. G. Roth, N. A. Romero and D. A. Nicewicz, Experimental and Calculated Electrochemical Potentials of Common Organic Molecules for Applications to Single-Electron Redox Chemistry, *Synlett*, 2016, **27**(05), 714–723.

76 I. Colomer, A. E. R. Chamberlain, M. B. Haughey and T. J. Donohoe, Hexafluoroisopropanol as a Highly Versatile Solvent, *Nat. Rev. Chem.*, 2017, **1**(11), 0088.

77 L. Eberson, M. P. Hartshorn, O. Persson and F. Radner, Making Radical Cations Live Longer, *Chem. Commun.*, 1996, **18**, 2105–2112.

78 N. Shida, Y. Imada, S. Nagahara, Y. Okada and K. Chiba, Interplay of Arene Radical Cations with Anions and Fluorinated Alcohols in Hole Catalysis, *Commun. Chem.*, 2019, **2**(1), 1–8.

79 D. Chong, M. Stewart and W. E. Geiger, Cycloaddition Reactions of Unactivated Olefins Catalyzed by an Organorhenium Electron-Transfer Mediator, *J. Am. Chem. Soc.*, 2009, **131**(23), 7968–7969.

80 M. P. Stewart, K. Lam, D. Chong and W. E. Geiger, CElectron-Transfer Catalyzed Cycloaddition Reactions of Unactivated Cyclic Olefins in Weakly Coordinating Anion Electrolyte, *J. Electroanal. Chem.*, 2015, **743**, 68–77.

81 R. A. Marcus, On the Theory of Oxidation-Reduction Reactions Involving Electron Transfer. I, *J. Chem. Phys.*, 1956, **24**(5), 966–978.

82 R. A. Marcus, On the Theory of Oxidation-Reduction Reactions Involving Electron Transfer. III. Applications to Data on the Rates of Organic Redox Reactions, *J. Chem. Phys.*, 1957, **26**(4), 872–877.

83 R. Marcus, On the Theory of Oxidation-Reduction Reactions Involving Election Transfer V. Comparison and Properties of Electrochemical and Chemical Rate Constants - Correction, *J. Phys. Chem.*, 2007, **67**(12), 2889.

84 N. S. Hush, Homogeneous and Heterogeneous Optical and Thermal Electron Transfer, *Electrochim. Acta*, 1968, **13**(5), 1005–1023.

85 R. Reslan, K. Lopata, C. Arntsen, N. Govind and D. Neuhauser, Electron Transfer beyond the Static Picture: A TDDFT/TD-ZINDO Study of a Pentacene Dimer, *J. Chem. Phys.*, 2012, **137**, 22–502.

86 H. X. Zhou and A. Szabo, Microscopic Formulation of Marcus' Theory of Electron Transfer, *J. Chem. Phys.*, 1995, **103**(9), 3481–3494.

87 J. Zwickl, N. Shenvi, J. R. Schmidt and J. C. Tully, Transition State Barriers in Multidimensional Marcus Theory, *J. Phys. Chem. A*, 2008, **112**(42), 10570–10579.

88 P. F. Barbara, T. J. Meyer and M. A. Ratner, Contemporary Issues in Electron Transfer Research, *J. Phys. Chem.*, 1996, **100**(31), 13148–13168.

89 S. F. Nelsen, R. F. Ismagilov, K. E. Gentile and D. R. Powell, Temperature Effects on Electron Transfer within Intervalence Bis(Hydrazine) Radical Cations, *J. Am. Chem. Soc.*, 1999, **121**(30), 7108–7114.

90 M. E. Walther and O. S. Wenger, Tuning the Rates of Long-Range Charge Transfer across Phenylene Wires, *ChemPhysChem*, 2009, **10**(8), 1203–1206.

91 D. H. Ess and K. N. Houk, Distortion/Interaction Energy Control of 1,3-Dipolar Cycloaddition Reactivity, *J. Am. Chem. Soc.*, 2007, **129**(35), 10646–10647.

92 F. M. Bickelhaupt and K. N. Houk, Analyzing Reaction Rates with the Distortion/Interaction-Activation Strain Model, *Angew. Chem., Int. Ed.*, 2017, **56**(34), 10070–10086.

93 F. M. Bickelhaupt, Understanding Reactivity with Kohn-Sham Molecular Orbital Theory: E2-SN2 Mechanistic Spectrum and Other Concepts, *J. Comput. Chem.*, 1999, **20**(1), 114–128.

94 I. Fernández and F. M. Bickelhaupt, The Activation Strain Model and Molecular Orbital Theory: Understanding and Designing Chemical Reactions, *Chem. Soc. Rev.*, 2014, **43**(14), 4953–4967.

95 L. P. Wolters and F. M. Bickelhaupt, The Activation Strain Model and Molecular Orbital Theory, *Wiley Interdiscip. Rev.: Comput. Mol. Sci.*, 2015, **5**(4), 324–343.

96 P. Vermeeren, S. C. C. van der Lubbe, C. Fonseca Guerra, F. M. Bickelhaupt and T. A. Hamlin, Understanding Chemical Reactivity Using the Activation Strain Model, *Nat. Protoc.*, 2020, **15**(2), 649–667.

97 K. Morokuma, Molecular Orbital Studies of Hydrogen Bonds. III. C═O···H–O Hydrogen Bond in $H_2CO\cdots H_2O$ and $H_2CO\cdots 2H_2O$, *J. Chem. Phys.*, 1971, **55**(3), 1236–1244.

98 T. Ziegler and A. Rauk, On the Calculation of Bonding Energies by the Hartree Fock Slater Method - I. The Transition State Method, *Theor. Chim. Acta*, 1977, **46**(1), 1–10.

99 M. von Hopffgarten and G. Frenking, Energy Decomposition Analysis, *Wiley Interdisciplinary Reviews: Computational Molecular Science*, John Wiley & Sons, Ltd, January 1, 2012, pp. 43–62.

100 I. Fernández, Combined Activation Strain Model and Energy Decomposition Analysis Methods: A New Way to Understand Pericyclic Reactions, *Phys. Chem. Chem. Phys.*, 2014, 7662–7671.

101 I. Fernández and F. M. Bickelhaupt, Origin of the "Endo Rule" in Diels-Alder Reactions, *J. Comput. Chem.*, 2014, **35**(5), 371–376.

102 T. A. Hamlin, B. J. Levandowski, A. K. Narsaria, K. N. Houk and F. M. Bickelhaupt, Structural Distortion of Cycloalkynes Influences Cycloaddition Rates Both by Strain and Interaction Energies, *Chem.–Eur. J.*, 2019, **25**(25), 6342–6348.

103 A. V. Marenich, C. J. Cramer and D. G. Truhlar, Universal Solvation Model Based on Solute Electron Density and on a Continuum Model of the Solvent Defined by the Bulk Dielectric Constant and Atomic Surface Tensions, *J. Phys. Chem. B*, 2009, **113**(18), 6378–6396.

104 J. Zhang, H. Zhang, T. Wu, Q. Wang and D. Van Der Spoel, Comparison of Implicit and Explicit Solvent Models for the Calculation of Solvation Free Energy in Organic Solvents, *J. Chem. Theory Comput.*, 2017, **13**(3), 1034–1043.

105 H. Zhang, T. Tan and D. Van Der Spoel, Generalized Born and Explicit Solvent Models for Free Energy Calculations in Organic Solvents: Cyclodextrin Dimerization, *J. Chem. Theory Comput.*, 2015, **11**(11), 5103–5113.

106 X. Chen, W. Qiao, W. Miao, Y. Zhang, X. Mu and J. Wang, The Dependence of Implicit Solvent Model Parameters and Electronic Absorption Spectra and Photoinduced Charge Transfer, *Sci. Rep.*, 2020, **10**(1), 1–8.

107 T. L. Cottrell, *The Strengths of Chemical Bonds*, Butterworths, London, 2nd edn, 1958.

108 S. W. Benson III, Bond Energies, *J. Chem. Educ.*, 1965, **42**(9), 502.

109 J. S. J. Tan and R. S. Paton, Frontier Molecular Orbital Effects Control the Hole-Catalyzed Racemization of Atropisomeric Biaryls, *Chem. Sci.*, 2019, **10**(8), 2285–2289.

110 O. Wiest, Structure and [2 + 2] Cycloreversion of the Cyclobutane Radical Cation, *J. Phys. Chem. A*, 1999, **103**(39), 7907–7911.

111 N. J. Saettel, J. Oxgaard and O. Wiest, Pericyclic Reactions of Radical Cations, *Eur. J. Org. Chem.*, 2001, **2001**(8), 1429–1439.

112 J. S. J. Tan, V. Hirvonen and R. S. Paton, Dynamic Intermediates in the Radical Cation Diels–Alder Cycloaddition: Lifetime and Suprafacial Stereoselectivity, *Org. Lett.*, 2018, **20**(10), 2821–2825.

113 During the preparation of this manuscript we became aware of related studies and we are very grateful to Prof. Hussein for sharing information with us, A. A. Hussein, A. Al-Yasari and Y. Ma, Thermodynamics Control Reactivity of Hypervalent Iodine-Mediated Styrene Hetero- and Homodimerization: Mechanistic Insights, 2020, DOI: 10.26434/chemrxiv.12350879.v4.

